Hyperoside attenuates non-alcoholic fatty liver disease in rats via cholesterol metabolism and bile acid metabolism

Songsong Wang [a,1], Feiya Sheng [a,1], Liang Zou [b], Jianbo Xiao [c,d,*], Peng Li [a,*]

[a] State Key Laboratory of Quality Research in Chinese Medicine, Institute of Chinese Medical Sciences, University of Macau, Macao 999078, China
[b] School of Medicine, Chengdu University, Chengdu 610106, China
[c] Institute of Food Safety and Nutrition, Jinan University, Guangzhou 510632, China
[d] Department of Analytical Chemistry and Food Science, Faculty of Food Science and Technology, University of Vigo, Vigo, Spain

GRAPHICAL ABSTRACT
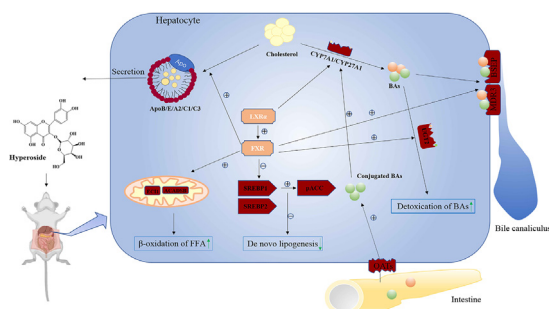
ARTICLE INFO

ABSTRACT

Introduction: Non-alcoholic fatty liver disease (NAFLD) results from increased hepatic total cholesterol (TC) and total triglyceride (TG) accumulation. In our previous study, we found that rats treated with hyperoside became resistant to hepatic lipid accumulation.

Objectives: The present study aims to investigate the possible mechanisms responsible for the inhibitory effects of hyperoside on the lipid accumulation in the liver tissues of the NAFLD rats.

Methods: Label-free proteomics and metabolomics targeting at bile acid (BA) metabolism were applied to disclose the mechanisms for hyperoside reducing hepatic lipid accumulation among the NAFLD rats.

Results: In response to hyperoside treatment, several proteins related to the fatty acid degradation pathway, cholesterol metabolism pathway, and bile secretion pathway were altered, including ECI1, Acnat2, ApoE, and BSEP, etc. The expression of nuclear receptors (NRs), including farnesoid X receptor (FXR) and liver X receptor α (LXRα), were increased in hyperoside-treated rats' liver tissue, accompanied by decreased protein expression of catalyzing enzymes in the hepatic *de novo* lipogenesis and increased protein level of enzymes in the classical and alternative BA synthetic pathway. Liver conjugated BAs were less toxic and more hydrophilic than unconjugated BAs. The BA-targeted metabolomics suggest that

hyperoside could decrease the levels of liver unconjugated BAs and increase the levels of liver conjugated BAs.

Conclusions: Taken together, the results suggest that hyperoside could improve the condition of NAFLD by regulating the cholesterol metabolism as well as BAs metabolism and excretion. These findings contribute to understanding the mechanisms by which hyperoside lowers the cholesterol and triglyceride in NAFLD rats.

© 2021 The Authors. Published by Elsevier B.V. on behalf of Cairo University. This is an open access article under the CC BY-NC-ND license (http://creativecommons.org/licenses/by-nc-nd/4.0/).

Introduction

Non-alcoholic fatty liver disease (NAFLD) is caused by increased liver fat accumulation in individuals not consuming excessive alcohol [1]; the incidence of NAFLD exceeds 30% in Western populations and could reach up to 88% in the obese [2,3].The pathogenesis of NAFLD experiences an evolution from "two hit theory" to "multiple hit model" theories. Since two hit theory has been proved to be too simplistic for recapitulating the complexity of human NAFLD, the widely accepted theory is the "multiple hit model", which suggests the development of NAFLD is related with many molecular pathways, involving hepatic fat accumulation, insulin resistance, necroinflammation and fibrosis induced by inflammatory cytokines and oxidative stress, and more widespread metabolic dysfunction because of the changes in crosstalk between different organs and tissues, such as the pancreas, liver, and gut [4].

Recently, studies have also demonstrated that gut microbiota, bile acids (BAs)[5–9], nuclear receptors (NRs) including farnesoid X receptor (FXR) and liver X receptors (LXRs) [10–14], and lipid metabolism also contribute to the development of NAFLD [15–17]. In addition, as a key regulator of BAs metabolism, FXR simultaneously plays an important role in regulating lipid and glucose metabolism, as well as BA homeostasis [10,11,14,18]. For example, hepatic de novo lipogenesis can be repressed by the activation of FXR, downregulating the master-regulator of sterol regulatory element binding protein 1c (SREBP1c). Hepatic TG accumulation and elevated levels of serum TG and cholesterol were also observed in mice lacking FXR [19]. Several studies also show that the activation of either chemosynthetic FXR agonist (GW4064) [20] or natural BAs could improve steatosis by inhibiting the SREBP1c and promoting β-oxidation of free fatty acids. Similarly with FXR, proteins that participate in fatty acid homeostasis, cholesterol homeostasis, and BAs metabolism are also encoded by the target genes of liver X-activated receptors (LXR) [13,18].

Emerging as potentially useful therapeutic agents for NAFLD, BA derivatives and compounds could influence BA-related signaling pathways from intestine and liver through the regulation of cholesterol secretion, metabolism of lipid, glucose and energy, and BA metabolism itself [5,6,9]. In the liver, the BAs are synthesized from cholesterol in the classical or neutral pathways, which are catalyzed by cholesterol 7a-hydroxylase (CYP7A1) and sterol-27-hydroxylase (CYP27A1) [7] respectively, and excreted into bile. BAs biosynthesis is one of the two major output pathways of cholesterol elimination; approximately 40% of cholesterol is eliminated in this way [21]. As a result, the inhibition of BAs biosynthesis will lead to cholesterol accumulation [22,23]. Recent studies have also shown that dysregulated BAs metabolism can affect lipid metabolism and is an important factor in the pathology of NAFLD. Besides, by activating or modulating BAs receptors, for example, FXR and Takeda G-protein-coupled receptor 5 (TGR5), the pathogenesis of NAFLD appears to be affected at multiple levels.

In NAFLD, the rate of fatty acid input (including *de novo* synthesis with subsequent esterification to triglycerides and fatty acid uptake) usually exceed the rate of fatty acid output (including secretion of very low-density lipoprotein (VLDL) and fatty acid oxidation) [24]. SREBPs are basic helix-loop-helix leucine zipper transcription factors, which can regulate the genes to govern cholesterol biosynthesis [25]. Cholesterol metabolism in the liver includes both cholesterol biosynthesis and efflux [26]. In NAFLD, dysregulation in the hepatic cholesterol metabolism is observed. For instance, the overexpression of SREBP-2 leads to enhanced hepatic cholesterol synthesis, changes in cholesterol absorption and secretion, and decreased BA synthesis, which in turn cause hepatic cholesterol accumulation [27]. Several genes that participate in lipogenesis, such as fatty acid synthase (FAS) and acetyl-CoA carboxylase (ACC), are also controlled by SREBPs [28,29].

Hyperoside, known as quercetin-3-O- galactoside (chemical constitution in Fig. 1), is a flavonol glycoside in a variety of herb medicines, such as *hawthorn*, *artemisia capillaris*, and *hypeticum perforatum* [30], processing anti-inflammatory, hepato-protective, antioxidant protective effects, etc. [31]. In our previous study, we found that rats treated with hyperoside were resistant to hepatic lipid accumulation, as shown in Fig. S1a–b, exhibiting the potential therapeutic effect for NAFLD. With the development of the liquid chromatograph-mass spectrometer (LC-MS), strategies of metabolomics and proteomics were widely applied in the researches of NAFLD [6,32–35]. Currently, label-free proteomics and BAs targeted metabolomics approaches have been employed to further determine the possible mechanisms responsible for the inhibitory effect of hyperoside on the lipid accumulation in the liver tissue of the NAFLD rat model. In the liver tissue of hyperoside-treated rats, we found that several proteins associated with the lipid metabolism pathway were altered and the expression of FXR and LXR increased, accompanied by decreased *de novo* lipogenesis and increased BAs synthesis. Besides, we also found that unconjugated BAs levels in the liver could be decreased and conjugated BAs levels in the liver could be increased through the treatment of hyperoside. In conclusion, hyperoside improves NAFLD in rats by regulating the cholesterol metabolism and BAs metabolism and excretion.

Experiment

Reagents

Hyperoside was supplied by the Nanjing SenBeiJia Biological Technology Co., Ltd. (NanJing, China) and the purity was 96% by HPLC. Antibody CYP7A1 (ab65596), CYP27A1 (ab126785), LXRα (ab176323), SREBP-1(ab28481), and SREBP-2(ab30682) were purchased from the Abcam company. Antibody ACC (3661S) and p-ACC (3676S) were offered by the Cell signaling company. Antibody FXR (417200) was provided by Thermo Fisher Scientific. All BAs standard substances were provided by Steraloids Inc. (Newport, RI, USA) and 10 stable isotope-labeled standard substances were supplied by Steraloids Inc. (Newport, RI, USA) and C/D/N
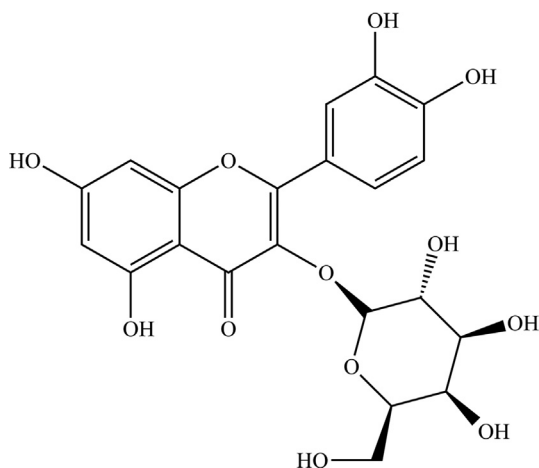
Fig. 1. The chemical structure of hyperoside.

Isotopes Inc. (Quebec, Canada). All standard substances were weighed accurately and dissolved in methanol, and the concentration of the individual stock solution was 5.0 mM. The mixed solution of individual BAs was prepared in a bile acid-free liver matrix and BAs calibrators at a concentration of 2500, 500, 250, 50, 10, 2.5, or 1 nM were obtained. Quality control samples at three different concentrations of 1500, 150, and 5 nM were prepared in BAFUM, respectively. Ten isotope-labeled bile acid internal standard substances were provided by Steraloids (Newport, RI, USA) and C/D/N Isotopes (Quebec, Canada). Internal standard (IS) concentrations were consistent to all the calibration points (150 nM for TCDCA-d9, GCA-d4, GCDCA-d4, TCA-d4, UDCA-d4, DCA-d4, CA-d4, GDCA-d4, β-CA-d5, and LCA-d4). Data quality was monitored and matrix effects were negated by IS.

Analytical grade ammonium acetate was provided by Sigma-Aldrich (St. Louis, MO, USA). Glacial acetic acid, methanol (Optima LC-MS), acetonitrile (Optima LC-MS), formic acid (Optima LC-MS), and isopropanol (Optima LC-MS) were supplied by Thermo-Fisher Scientific (FairLawn, NJ, USA). Mill-Q Reference system coupled with a LC-MS Pak filter (Millipore, Billerica, MA, USA) was used for the ultrapure water.

Animals

Animal experiments are consistent with previous experiments. In brief, wistar male rats aged 10 weeks (220–250 g) were supplied by Chengdu DaShuo Experimental Animal Co., Ltd. All animals were fed in the animal facility of the College of Pharmacy and Biological Engineering, ChengDu University, Cheng Du, China. All rats were raised individually in a ventilative squirrel-cage (humidity 60 ± 5%, 22 ± 2 °C, 12 h light/dark cycle). A basic diet or defined diet was supplied to all animals and all rats had free access to the water.

Animal experiments procedure

The experimental animals were divided into a blank group, a model group, a high dosage hyperoside group (1.5 mg/kg/day), and a low dosage hyperoside group (0.6 mg/kg/day). The blank group was fed with a basal diet and the rats in the model group were fed with the high fat diet mentioned below. The other two groups were fed with the high fat diet but were supplemented with hyperoside at a dosage of 1.5 and 0.6 mg/kg body weight per day by oral administration for 20 days. The same volume of water was administered to the blank and model groups.

The high fat diet was provided by TROPHIC Animal Feed High-Tech Co. Ltd, Nanjing, China. The high fat diet contained 65.55% basal diet, 20% lard oil, 10% sucrose, 4% cholesterol, 0.25% cholate, and 0.2% methylthiouracil and was stored in 4 °C in a refrigerator before use. After the final administration, 10% chloral hydrate was used for the anesthesia of the rats; the liver was taken and stored in −80 °C in a refrigerator for use.

Ethics statement

The animal experiments were conducted in accordance with the ethical policies and procedure authorized by the laboratory animal ethics committee, University of Macao (Approved No. UMARE-013-2016).

Protein extraction of liver tissue for western blot analysis

The total protein of liver tissue was extracted on ice following the steps below: a liver sample (50 mg) was placed in a glass homogenizer, a 500 μl of RIPA buffer containing 1% phenylmethyl-sulfonyl fluoride (PMSF) was added and ground to form a homogenate on ice, which was then transferred to a 2 mL EP tube for the ultrasound, shook for 2–3 s and repeated 3–5 times, then centrifuged at 12000 rpm for 30 min. Approximately 1/4 vol of 5-fold loading buffer was added and then the liver was heated in a boiling water bath for 5 min to denature the protein before spotting the sample.

Western blot analysis of liver tissue

A separation of the same amounts of proteins (30 μg) was carried out using SDS polyacrylamide gel electrophoresis and then this was transformed to a poly vinylidene difluoride filters membrane. Nonfat milk with TBST (5%) was used for the membranes block for one hour and the first antibodies were hatched within the membranes overnight at 4 °C. The membranes were incubated with the second antibody for one hour after the cleanout of the membranes three times with TBST. In addition, GAPDH was used as a loading control. ECL reagents were added and the band intensity was detected by Bio-Rad ChemiDoc™ Touch Imaging System. Western blotting analysis was carried out using the published method [36].

Extraction of proteins for label-free proteomics

The extraction of proteins in the liver followed the previous methods with minor changes [37]. The SDT buffer (4 %SDS, 100 mM Tris-HCl, pH 7.6) was added before being transferred to the tubes. The homogenization of lysate was carried out by MP Fastprep-24 Automated Homogenizer for 30 s, twice. The sonication of the liver tissue homogenate was carried out and then boiled in water for 15 min after being centrifuged. 0.22 μm filters were used to filter the supernatant. The quantification of protein was operated using the BCA Protein Assay Kit (P0012, Beyotime). The sample was stored at −20 °C for use.

A 6X loading buffer was used for the admixture of the proteins (20 μg) of each sample respectively, followed by boiling in water for 5 min, then being separated on 12.5% SDS-PAGE gel; the visualization was performed using Coomassie Blue R-250 staining. Proteins (200 μg) of each sample were reduced with 50 mM DTT for 30 min at 56 °C. The low-molecular-weight components, DTT and UA buffer, were used for the dislodgment of detergent. The blockage of reduced cysteine residues was carried out, subsequently, incubation of the samples was performed in darkness for 30 min. A 100 μl UA buffer was applied to wash the filters three times and then a 100 μl 25 mM NH_4HCO_3 buffer was used, twice. Finally,

the digestion of the protein suspensions was manipulated overnight at 37 °C, and the consequent peptides were gathered as a filtrate.

Easy nLC-MS analysis of label-free proteomics

Desalinization of the peptide was actualized using C18 Cartridges, which was subsequently condensed by vacuum centrifugation and redissolved in 40 μl formic acid (0.1%, v/v). UV light spectral density was used for the estimation of peptide content at 280 nm. Separation of proteins was performed on Easy nano LC from Thermo Fisher Scientific and was used for the separation of proteins, followed by a MS/MS analysis that was carried out using a Q Exactive Plus mass spectrometer from Thermo Fisher Scientific. The separation of 2 μg peptide was implemented by the C18-reversed phase analytical column (Acclaim PepMap RSLC 50 μm × 15 cm, nano viper, P/N164943) from Thermo Fisher Scientific and a linear grading of buffer B (80% acetonitrile and 0.1% formic acid) was used and the flow rate was 300 nl/min. The gradient was the following: 0–5 min, 5% B; 5–90 min, 5–28% B; 90–105 min, 28–38% B; 105–110 min, 38–100% B; 110–115 min, 100% B. For the acquisition of MS data, the most abundant precursor ions were chosen for the HCD fragmentation. MS1 scans were acquired at a resolution of 70,000 at m/z 200 with an AGC target of $3e^6$ and a maxIT of 50 ms. MS2 scans were acquired at a resolution of 17,500 at m/z 200 with an AGC target of $2e^5$ and a maxIT of 45 ms, and isolation width was 2 m/z. Only ions with a minimum intensity of $2e^3$ and the fragmentation chose a charge state between 2 and 6. Dynamic exclusion for selected ions was 30 s. Normalized collision energy was 27 eV.

KEGG and GO analysis for label-free proteomics

All protein sequences were aligned to homosapiens; the database was downloaded from NCBI (ncbi-blast-2.2.28 + win32.exe) and only the sequences E-value <= $1 e^{-3}$ and those in the top 10 were kept. Secondly, the GO terms (database version: go_201504.obo) of the sequence with the top Bit-Score were selected by Blast2GO. The annotation from GO terms to proteins was completed by Blast2 GO Command Line. ANNEX was used for the further improvement of annotation and connection between GO terms. Fisher's Exact Test was carried out to enrich the GO terms via comparing the numbers of differentially expressed proteins and total proteins correlated to GO terms.

The pathway analysis was performed using the KEGG database. Significantly enriched pathways were identified using Fisher's Exact Test and by comparing the number of differentially expressed proteins and total proteins correlated to pathways. This proteomics experiment was supported by LC-BIO Technologies CO., LTD. Hangzhou, China.

Pretreatment of liver tissue in metabolomic analysis

The pretreatment was implemented according to the previously reported methods [38]. In brief, 10 mg of tissue were weighed accurately into an Eppendorf centrifuge tube with a safety clasp, then approximately 25 mg of pre-cooled grinding beads and 20 μl of ultrapure water were added, and mixed with a homogenizer. 180 μl of acetonitrile/methanol (v/v = 8:2) mixed solvent containing 10 μl of IS was added to the centrifuge tube. After homogenization, this was centrifuged at 13,500 rpm for 20 min at 4 °C. After centrifugation was completed, a 96-well plate was used for the transfer of the supernatant and this was further lyophilized in a freeze dryer equipped with a stop tray system. The dried actual sample, standard curve, and quality control sample powder were redissolved using a 1:1 mixture of

methanol / acetonitrile (20/80) and ultrapure water and were centrifuged at 13,500 rpm for 20 min at 4 °C. Similarly, a 96-well plate was used for the transfer of the supernatant and to wait for injection analysis. The injection volume was 5 μl.

Bile acids quantification

The XploreMET platform (Metabo-Profile, Shanghai, China) manipulated the BAs targeted metabolomics profiling. In the present study, the quantification of BAs was carried out using ultra-performance liquid chromatography coupled with the tandem mass spectrometry (UPLC-MS/MS) system (ACQUITY UPLC-Xevo TQ-S, Waters Corp., Milford, MA, USA). Chromatographic conditions and mass spectrometry conditions were described as follows. Columns ACQUITY UPLC Cortecs C18 1.6 μM VanGuard pre-column (2.1 × 5 mm) and ACQUITY UPLC Cortecs C18 1.6 μM analytical column (2.1 × 100 mm) were used for the separation of BAs. The column temperature was 30 °C. Water with formic acid (pH = 3.25) was chosen as mobile phase A and methanol/acetonitrile (20:80) were chosen as mobile phase B, respectively. The flow rate was 0.40 mL/min and the injection volume was 5 μl. The mobile phase gradient was: 0–1 min, 5% B; 1–3 min, 5–30% B; 3–15 min, 30–100% B; 15–16 min, 100–5% B; 16–17 min, 5% B. The mass capillary voltage was 2.0 Kv, the desolvation gas flow was 1000 L/Hr, the desolvation temperature was 550 °C, and the source temperature was 150 °C.

When storage in −20 °C in the freezer overnight was finished, the extraction solvents were added to the thawed samples immediately. An ice-salt bath was used to minimize sample degradation and to keep the temperature of the samples low during sample preparation. Every ready sample should be detected within 48 h.

Three types of QC samples including test mixtures, stable isotope-labelled IS, and three different levels (low, middle, and high) quality controls and solvent blank samples were routinely used in our study. Peak signal intensity, chromatographic peak shape, and retention time stability were evaluated to ensure that the instruments were performing well. The retention time shift for a batch of all samples should be less than 4 s and the variety in peak intensity should be less than 15%. BAs in the liver were quantified based on the previously established method [39].

Data analysis

MaxQuant software version 1.5.5.1 was used for the analysis of the MS data. MS data were raked through the Uniprot_RattusNorvegicus_36141_20200306 database. A deviation of 6 ppm was set for the initial search, following an enzymatic cleavage rule of Trypsin/P and allowing for a maximal of two missed cleavage sites and a deviation of 20 ppm for fragment ions. Fixed modification was defined using the carbamidomethylation of cysteines, while simultaneously, methionine oxidation and protein N-terminal acetylation were deemed as variable modifications. For the identification of peptide and protein, a cutoff of the global FDR was set to 0.01. Protein abundance was counted based on the normalized spectral protein intensity (LFQ intensity). Proteins with fold changes FC > 1.2 or <0.83 and p value (student's t test) <0.05 were considered as differential expression proteins.

The bar plots in our study were generated using GraphPad Prism 8.0 and the data were expressed as means ± standard error of mean (SEM). The single-dimensional Anova test or Kruskal-Wallis (K-W test) test were applied and values of p< 0.05 and p< 0.01 were deemed as significant. QuanMET software (v1.0, Metabo-Profile, Shanghai, China) was used for the peak integration, calibration, and metabolite quantitation. The powerful package R studio was applied to the statistical analysis. The Image Lab software was used for the western blotting strip detection.

Results

Effects of hyperoside treatment on liver tissue proteins expression

The liver protein profiles of hyperoside treatment rats were clarified using the liver samples from the rats treated with hyperoside by nanoLC-MS. For comparison of the protein profiles, our result revealed that 2329 proteins were identified (MaxQuant software) and showed a total of 75 significant change protein peaks (FC > 1.2 or < 0.83, and p < 0.05) between the hyperoside treatment group (n = 4) and the model group (n = 4), including 33 upregulated proteins and 42 downregulated proteins, as shown in Fig. 2a and supplemental Table S1. To inquire into the nature of these proteins with significant changes, a GO (www.geneontology.org) enrichment analysis based on classification was applied to identify the biological mechanisms of significant changes in the proteins. The classification analysis of the cellular component (p < 0.05) showed that the proteins are mainly related to very low-density lipoprotein particles, etc. In the molecular function analysis (p < 0.05), the result indicated that differentially changed proteins were leukotriene-C4 synthase activity related, etc. The biological processes category analysis (p < 0.05) result showed the proteins mainly involved in lipoprotein metabolic process, etc., as shown in Fig. 2c.

A Kyoto Encyclopedia of Genes and Genomes (KEGG) enrichment analysis was carried out to find important complement pathway proteins using the differential proteins. The top 18-ranking authoritative KEGG pathways (p < 0.05) are biosynthesis of unsaturated fatty acids, cell cycle, fatty acid degradation, naphthalene degradation, valine, leucine and isoleucine degradation, primary bile acid biosynthesis, peroxisome, bile secretion, cholesterol metabolism, ferroptosis, tyrosine metabolism, glutathione metabolism, African trypanosomiasis, malaria, retinol metabolism, chemical carcinogenesis, metabolism of xenobiotics by cytochrome P450, and drug metabolism, as shown in Fig. 2b.

Based on the published literature on NAFLD, what stands out in the KEGG analysis are the following pathways: fatty acid degradation (p < 0.05), primary bile acid biosynthesis (p < 0.05), bile secretion (p < 0.05), and cholesterol metabolism (p < 0.05). In the fatty acid degradation pathway, the proteins expression required for fatty acid β-oxidation were elevated obviously in the hyperoside group, which increased in comparison with the model group, including Delta3-Delta2-enoyl-CoA delta isomerase (FC = 1.19; p = 0.0145) and short/branched chain specific acyl-CoA dehydrogenase (FC = 1.36; p = 0.0281). This revealed that up-regulating fatty acid β-oxidation played an essential role in NAFLD treatment by hyperoside. Two enzymes participated in ethanol oxidation including alcohol dehydrogenase 4 (Class II) (FC = 1.83; p = 0.0005) and alcohol dehydrogenase 5 (FC = 1.47; p = 0.0008), which were also found to be elevated after the hyperoside treatment. In contrast, the protein of Acyl-coenzyme A oxidase (FC = 0.67; p = 0.0098) was shown to be down-regulated upon hyperoside therapy. In the bile secretion pathway, the hyperoside group showed increased expression of 6 proteins including solute carrier family 22 member 7 (FC = 1.30; p = 0.0344), UDP-glucuronosyltransferase (FC = 1.66; p = 0.0067), Glucuronosyl-
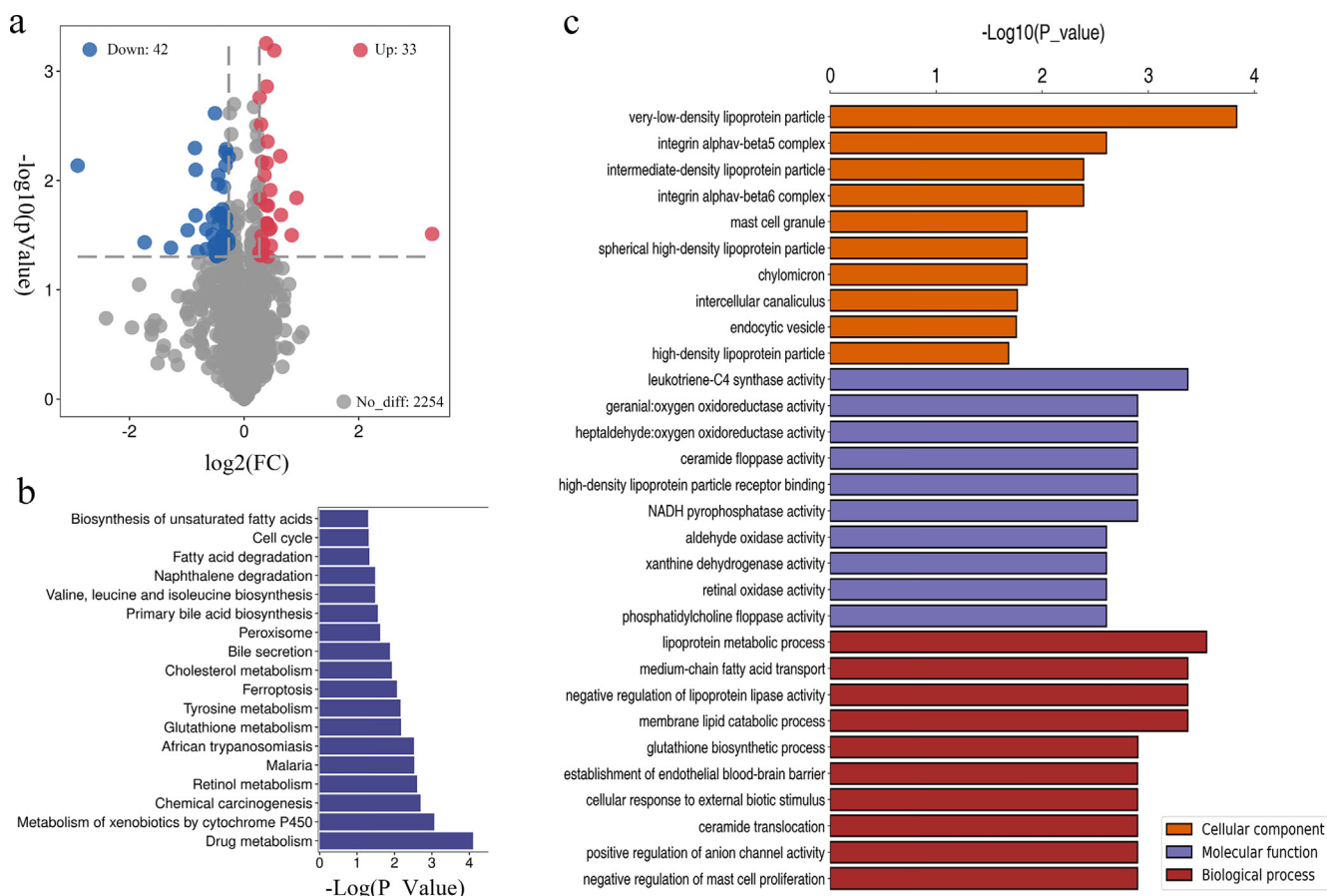
Fig. 2. Proteomics analysis between model and hyperoside group. (a) Volcano map of differential protein. FC > 1.2 or < 0.83, and p < 0.05. (b) KEGG enrichment analysis differential protein between model and hyperoside group (p < 0.05). (c) GO enrichment analysis of differential protein between model and hyperoside group (p < 0.05).

Table 1

The differential proteins between model and hyperoside group involved in bile secretion, fatty acid degradation, and cholesterol metabolism pathways.

Pathway	Protein IDs	Gene Name	Peptides	Razor + unique peptides	Unique peptides	Sequence coverage [%]	Definition	Fold change (Hyperoside/Model)	P Value
Bile secretion	Q5RLM2	SLC22A7, OAT2	6	6	6	14.6	MFS transporter, OCT family, solute carrier family 22 (organic anion transporter), member 7	1.30	0.0344
	Q68G19	Ugt2b35	19	2	2	43.2	UDP-glucuronosyltransferase	1.66	0.0067
	D4A132	Ugt2b10	14	2	2	28.6	Glucuronosyltransferase [EC:2.4.1.17]	1.24	0.0287
	Q5FVR5	Acnat2	11	11	11	36.1	Bile acid-CoA:amino acid N-acyltransferase [EC:2.3.1.65 3.1.2.2]	0.59	0.0259
	A0A2P1EA62	Abcb11	38	38	37	38.1	Bile salt export pump	1.44	0.0006
	Q08201	Abcb4	10	9	7	10.3	Phosphatidylcholine translocator ABCB4	1.38	0.0272
	P09875	Ugt2b1	25	3	0	50.4	UDP-glucuronosyltransferase 2B1	1.22	0.0484
Fatty acid degradation	P23965	ECI1, DCI	14	14	1	48.1	Delta3-Delta2-enoyl-CoA isomerase [EC:5.3.3.8]	1.19	0.0145
	P70584	ACADSB	15	15	15	51.2	Short/branched chain acyl-CoA dehydrogenase [EC:1.3.99.12]	1.36	0.0281
	A1L128	Adh4	19	4	4	81.2	Alcohol dehydrogenase 4 [EC:1.1.1.1]	1.83	0.0005
	Q7TQ90	Adh4	31	31	0	49.5	S-(hydroxymethyl)glutathione dehydrogenase/alcohol dehydrogenase 5 [EC:1.1.1.284 1.1.1.1]	1.47	0.0008
	F1M609	Acox1	29	1	1	74.1	Acyl-CoA oxidase [EC:1.3.3.6]	0.67	0.0098
Cholesterol metabolism	P02650	ApoE	21	21	21	67.6	Apolipoprotein E	1.36	0.0117
	P19939	ApoC1	3	3	3	28.4	Apolipoprotein C-I	1.44	0.0020
	P04638	ApoA2	5	5	5	59.8	Apolipoprotein A-II	1.38	0.0123
	A0A2P1EA62	Abcb11	38	38	37	38.1	Bile salt export pump	1.44	0.0006
	A0A0G2K8Q1	ApoC3	2	2	2	39	Apolipoprotein C-III	1.31	0.0168
	Q63052	ApoB	114	114	114	33.3	Apolipoprotein B	1.23	0.0321

Protein IDs, identifier(s) of protein(s) contained in the protein group; Number of proteins, number of proteins contained within the group; Peptides, Peptides, the total number of peptide sequences associated with the protein group; Razor + unique peptides, the total number of razor + unique; Unique peptides, the total number of unique peptides associated with the protein group; Sequence coverage [%], Percentage of the sequence that is covered by the identified peptides of the best protein sequence contained in the group; Definition, name of target protein in KEGG database; FC, fold change of hyperoside group/Model group; P value, P value of hyperoside group vs Model group.
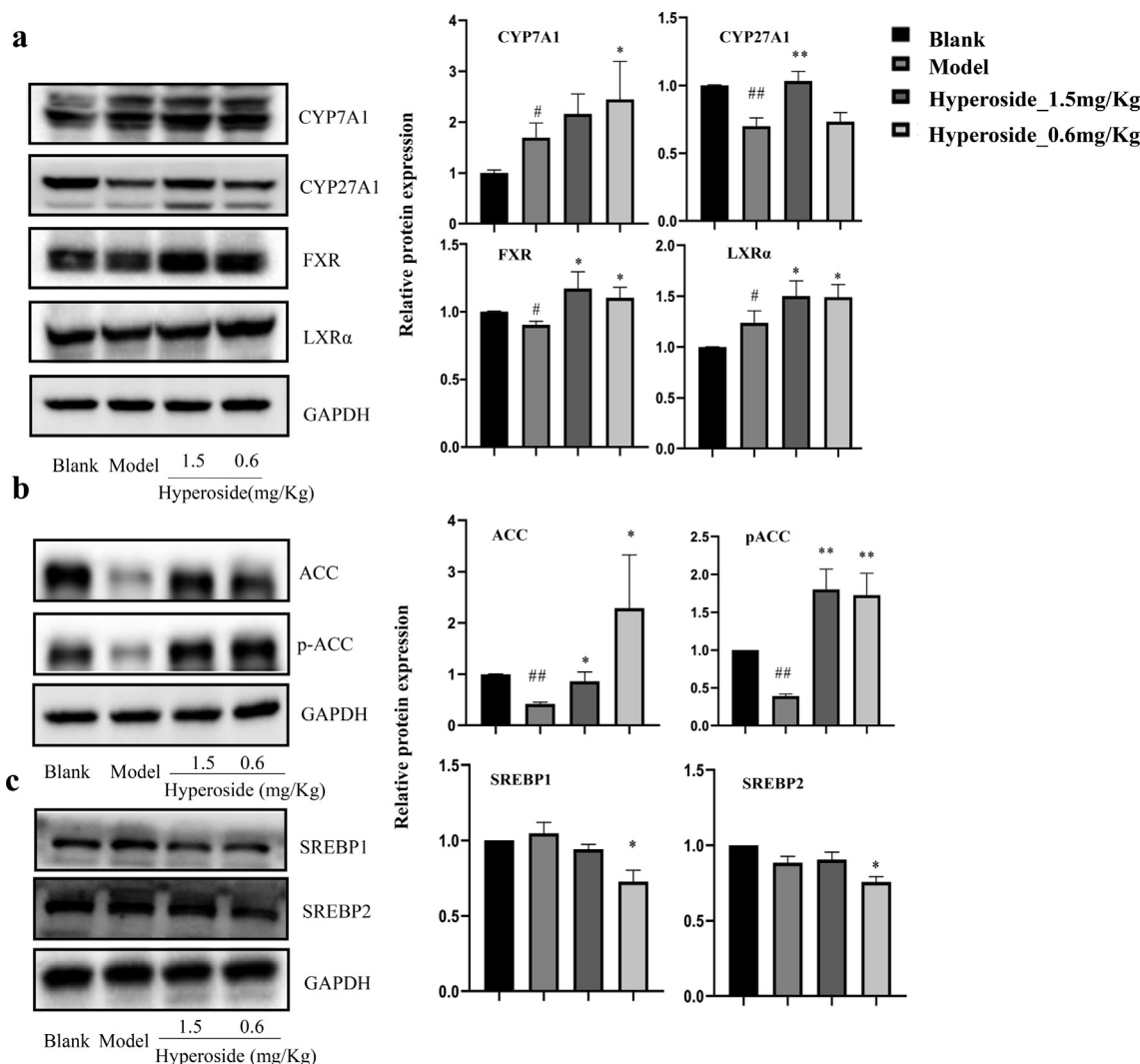
Fig. 3. Hyperoside treatment increases the expression of proteins involved in bile acid biosynthesis, increases the expression of nuclear receptors, and decreases the expression of proteins involved in *de novo* lipogenesis. **a.** The protein expression of CYP7A1, CYP27A1, FXR, and LXRα, GAPDH was chosen as a loading control, and the density of the signals for CYP7A1, CYP27A1, FXR, and LXRα. **b.** The protein expression of ACC and pACC, GAPDH was chosen as a loading control, and the density of the signals for ACC and pACC. **c.** The protein expression of SREBP1 and SREBP2, GAPDH was chosen as a loading control, and the density of the signals for SREBP1 and SREBP2. n = 3, data are presented as mean ± SEM. ##, $p < 0.01$, #, $p < 0.05$, by unpaired Student t test compared with blank group, **, $p < 0.01$, *, $p < 0.05$, by unpaired Student t test compared with model group.

transferase (FC = 1.24; p = 0.0287), Bile salt export pump (BSEP) (FC = 1.44; p = 0.0006), Phosphatidylcholine translocator ABCB4 (FC = 1.38; p = 0.0272), and UDP-glucuronosyltransferase 2B1 (FC = 1.22; p = 0.0484). Notably, the BSEP (BSEP, ABCB11) had the basic features of promoting the excretion of BAs from hepatic cell into bile; UDP-glucuronosyltransferase explained the conjugation and detoxification of BAs. Acyl-coenzyme an amino acid N-acyltransferase 2, which effectively conjugates both long-chain fatty acids and very long-chain fatty acids to taurine, was downregulated in the hyperoside treatment group.

In the cholesterol metabolism, all detected proteins levels increased evidently in the hyperoside treatment group, including Apolipoprotein E (FC = 1.36; p = 0.0117), Apolipoprotein C-I (FC = 1.44; p = 0.0020), Apolipoprotein A-II (FC = 1.38; p = 0.0123), BSEP (FC = 1.44; p = 0.0006), Apolipoprotein C-III (FC = 1.31; p = 0.0168), and Apolipoprotein B (FC = 1.23; p = 0.0321), indicating that hyperoside treatment promotes cholesterol efflux in rats' hepatocytes. The details are given in Table 1.

Bile acids synthesis and nuclear receptors activity are changed after hyperoside treatment

To further explore mechanism of hyperoside reducing lipid accumulation in a rat liver, the protein expression of hepatic *de novo* lipogenesis markers ACC, p-ACC, SREBP1, and SREBP2, enzymes involved in BA synthesis, including CYP7A1 and CYP27A1, and nuclear receptors, including FXR and LXRα, were measured in the blank, model, and hyperoside treatment groups. It can be seen in Fig. 3, compared to the model group, the expression levels of protein CYP7A1 after the hyperoside treatment were increased, especially in the 0.6 mg/kg hyperoside treatment group (p < 0.05), and CYP27A1 in 1.5 mg/kg hyperoside-treated rats were observably increased (p < 0.01) compared to the model group, revealing that conversion from cholesterol to BAs was also increased. In line with this, the protein expression levels of FXR and LXRα were also elevated observably (p < 0.05) in rats treated with the hyperoside supplement.

Table 2
The 23 bile acids content in liver analyzed in our study.

Class	Full name	Abbreviation	Blank	Model	Hyperoside (1.5 mg/Kg)	Hyperoside (0.6 mg/Kg)
Secondary / Conjugated BAs	Tauro-ω-muricholic acid	TωMCA	8.87 ± 1.45	1.25 ± 0.58##	3.05 ± 1.46	1.93 ± 1.14
Secondary /Conjugated BAs	Tauro-α-muricholic acid	TαMCA	8.50 ± 0.74	10.54 ± 0.35##	12.6 ± 1.01*	9.36 ± 2.31
Secondary /Conjugated BAs	Tauro-β-muricholic acid	TβMCA	35.68 ± 9.49	13.29 ± 3.25#	15.97 ± 3.10	13.08 ± 0.92
Primary /Conjugated BAs	Taurocholic acid	TCA	23.41 ± 8.56	15.22 ± 5.20	24.59 ± 4.76*	17.68 ± 2.97
Secondary /Conjugated BAs	Tauroursodeoxycholic acid	TUDCA	1.73 ± 0.31	1.15 ± 0.05#	1.39 ± 0.20*	0.96 ± 0.18
Secondary /Conjugated BAs	Taurohyodeoxycholic acid	THDCA	34.03 ± 6.26	1.12 ± 0.75##	1.64 ± 0.40	1.79 ± 0.62
Primary /Conjugated BAs	Taurochenodeoxycholate	TCDCA	6.54 ± 1.74	9.38 ± 0.53#	12.09 ± 3.28	7.99 ± 0.77*
Secondary /Conjugated BAs	Taurodeoxycholate	TDCA	16.18 ± 0.91	22.93 ± 1.15##	33.49 ± 8.34*	42.7 ± 21.95
Secondary/Unconjugated BAs	ω-muricholic acid	ωMCA	0.64 ± 0.33	8.03 ± 2.94##	5.31 ± 1.54	2.92 ± 1.12*
Secondary/Unconjugated BAs	3β-Cholic Acid	βCA	0.07 ± 0.01	0.84 ± 0.55	0.79 ± 0.47	0.80 ± 0.50
Secondary/Unconjugated BAs	α-muricholic acid	αMCA	0.79 ± 0.53	42.95 ± 18.75#	24.63 ± 4.72	18.86 ± 15.06
Secondary/Unconjugated BAs	β-muricholic acid	βMCA	1.78 ± 1.14	17.45 ± 6.39##	9.59 ± 3.65*	7.89 ± 4.50*
Secondary/Unconjugated BAs	Allocholic acid	ACA	0.14 ± 0.05	1.06 ± 0.17##	0.37 ± 0.17**	0.37 ± 0.26**
Primary/Unconjugated BAs	Cholic acid	CA	2.58 ± 2.60	75.14 ± 35.62#	58.71 ± 45.27	43.78 ± 36.06*
Secondary/Unconjugated BAs	Murocholic acid	muroCA	0.07 ± 0.01	0.30 ± 0.13#	0.23 ± 0.12	0.17 ± 0.03
Secondary/Unconjugated BAs	Ursodeoxycholic acid	UDCA	0.26 ± 0.11	5.15 ± 2.02##	2.10 ± 0.41*	1.94 ± 1.78*
Secondary/Unconjugated BAs	α-hyodeoxycholic acid	HDCA	3.87 ± 2.48	8.39 ± 2.75	4.88 ± 1.67	5.94 ± 3.98
Primary/Unconjugated BAs	Chenodeoxycholic acid	CDCA	0.29 ± 0.26	27.69 ± 11.41##	10.81 ± 1.02*	9.05 ± 7.88*
Secondary/Unconjugated BAs	Deoxycholic acid	DCA	0.52 ± 0.37	30.97 ± 12.37##	21.07 ± 3.14	20.10 ± 19.00
Secondary/Unconjugated BAs	Lithocholic acid	LCA	0.13 ± 0.08	2.55 ± 0.87##	1.42 ± 0.35	0.86 ± 0.35*
Secondary/Unconjugated BAs	7-ketolithocholic acid	7-Keto-LCA	0.01 ± 0.00	0.19 ± 0.08#	0.05 ± 0.01*	0.05 ± 0.04*
Secondary/Unconjugated BAs	6-ketolithocholic acid	6-Keto-LCA	0.02 ± 0.01	0.05 ± 0.02	0.03 ± 0.01*	0.04 ± 0.03
Secondary/Unconjugated BAs	NorCholic acid	NorCA	0.03 ± 0.01	0.08 ± 0.02##	0.07 ± 0.02	0.07 ± 0.05

##, $p < 0.01$, #, $p < 0.05$, by unpaired Student t test compared with blank group. **, $p < 0.01$, *, $p < 0.05$, by unpaired Student t test compared with model group.

The protein expression levels of ACC and pACC in the model group were obviously down-regulated ($p < 0.01$) in comparison with the blank group and the model group. These two enzymes were significantly increased (ACC, $p < 0.05$; p-ACC, $p < 0.05$) after hyperoside feeding, suggesting that the hyperoside treatment caused ACC phosphorylation in the liver. As key lipogenic transcription factors, SREBP-1 that connected with fatty acid and TG synthesis, and SREBP-2 that was involved in the synthesis of cholesterol were highly expressed in the liver. The protein expression of SREBP-1 was evidently descended ($p < 0.05$) in the 0.6 mg/kg hyperoside treatment group in comparison to model group, and the SREBP-2 was obviously down-regulated ($p < 0.05$) only in the 0.6 mg/kg hyperoside treatment group compared to the model group. The triplicates of all western blots are illustrated in Fig. S2.

Alterations of bile acid metabolism in hyperoside treatment rats

Genomics and proteomics let us know what might happen, though metabolomics tells us what did actually happen. In order to better understand the role of hyperoside in alleviating NAFLD, a BAs targeted metabolomics analysis was performed. The changes of 23 BAs, as displayed in Table 2, including 2 primary BAs and their taurine conjugated forms, 6 secondary BAs and their taurine conjugated forms, and 7 individual secondary BAs from hepatic tissue between four groups was investigated using PCA and PLS-DA analysis, as shown in Fig. 4a and 4b. A clear separation was observed between the blank and the model groups, indicating that the NAFLD model in rats was successfully established, supporting the potential role for hyperoside in the prevention and treatment of NAFLD in rats. Permutation was used for the model validation of PLS-DA. As shown in Fig. 4c, values of R^2 and Q^2 were 0.257 and −0.28 respectively, indicating that the model with the higher goodness of fit was obtained. As a result, the disorder BAs metabolism was observed after the treatment with the high-fat diet, and the dysregulation BAs metabolism was attenuated by the hyperoside treatment. From the loading plot (PLS-DA), the BAs with VIP value > 1 contribute significantly to the PLS-DA model. As exhibited in Fig. 4d, 8 BAs with VIP value > 1, including THDCA, TβMCA, CDCA, βMCA, αMCA, DCA, CA, and TDCA showed a significant difference between the four groups.

According to the normality of the data and the homogeneity of variance, a single-dimensional Anova test or K-W test was also applied to the discovery of BAs with significant contribution to the differentiation of four groups. The differential metabolite threshold is set as: $p < 0.05$. Further statistical tests revealed that 15 BAs were highlighted. The boxplot with points and a heat map with a Z score of the 15 BAs are shown in Fig. 5a and 5b. As can be seen from the figure, two primary BAs, CA and CDCA, and 10 secondary BAs, LCA, 7-Keto-LCA, muroCA, UDCA, ωMCA, norCA, αMCA, DCA, βMCA, and ACA were elevated after the treatment with a high-fat diet. The other 3 conjugated BAs, TωMCA, THDCA, and TβMCA were down-regulated in the model group. Compared to the model group, the administration of hyperoside decreased the unconjugated primary BAs and unconjugated secondary BAs levels in the rats and increased the levels of conjugated bile acids including TωMCA, THDCA, and TβMCA in the rats.

All 23 BAs' content in the liver are shown in Table 2. The levels of other taurine-conjugated BAs, including TαMCA, TCA, TUDCA, TCDCA, and TDCA were also raised ($p < 0.05$) in hyperoside-treated rats in comparison to the model group rats. High-fat diets contributed to the up-regulated concentration of total unconjugated BAs in rats, about 12 times higher than the blank group ($p < 0.01$) and treatment with hyperoside decreased the levels of total unconjugated BAs ($p < 0.05$). On the contrary, it is of interest that the hyperoside reversed the down-regulated total taurine-conjugated BAs caused by the high-fat diet in the rats ($p < 0.01$). The results are exhibited in Fig. 6a and 6b. The other 3 secondary BAs, including 6-Keto-LCA, βCA, and HDCA all increased in the high-fat diet-fed rats and were down-regulated by the hyperoside treatment.

Discussion

In our study, several lines of evidence have been presented to support the hypothesis that hyperoside treatment enhances the bile secretion pathway, the fatty acid degradation pathway, the cholesterol metabolism pathway, BAs biosynthesis and metabolism, and the expression of nuclear receptors (FXR, LXRα). It restrains the *de novo* lipogenesis in rats, helping us to understand the mechanisms underlying hyperoside obviously reducing hepatic
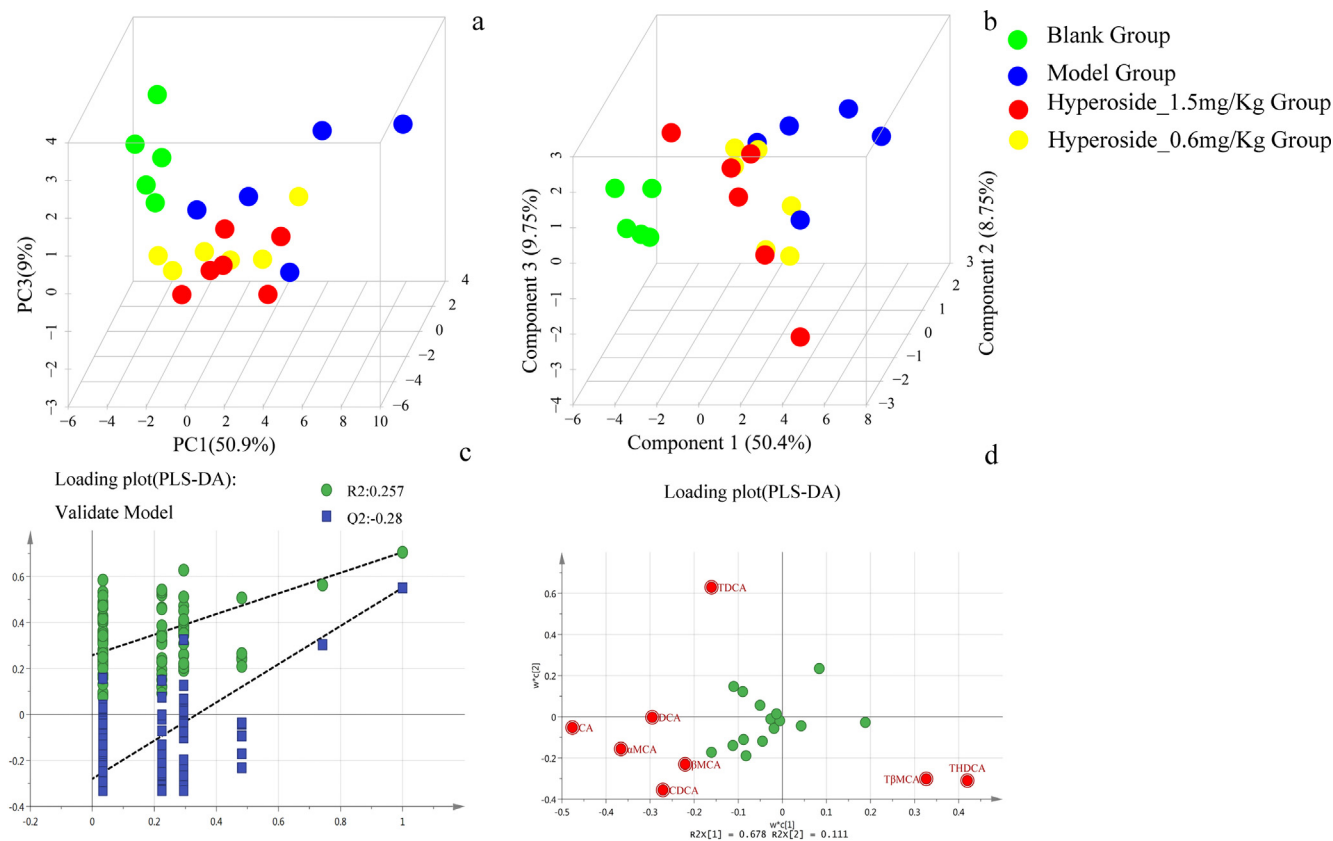
Fig. 4. The enhanced PCA and PLS-DA model for discrimination between blank, model and hyperoside groups. **a.** Score plot of the 3D PCA-DA model **b.** Score plot of the 3D PLS-DA model. **c.** Statistical validation of the PLS-DA model by permutation testing (n = 300) [Q^2 = −0.28, R^2 = 0.257]. **d.** Loading plot created from OPLS-DA modeling; red ball indicates BAs with VIP value greater than 1.

TC and TG levels. In fatty acid metabolism, the inhibition of ACC simultaneously stimulates fatty acid oxidation and inhibits fatty acid synthesis [24,40]. In our study, the phosphorylation of ACC was induced by the hyperoside treatment, opening up the possible mechanisms of hyperoside inhibiting the fatty acid synthesis by decreasing the synthesis of malonyl CoA and stimulating fatty acid oxidation [36,41] in the liver. Consistent with the protein expression of ACC, the protein expression of SREBP-1, which is a lipogenesis master regulator and participates in the transcriptional activation of ACC [42 25], was reduced by hyperoside. In addition, in comparison with the rats in the model group, elevated plasma TG levels were observed in rats feeding hyperoside, which may be also associated with the inhibition of ACC [24]. The results of ACC and SREBP-1 are consistent with the aforementioned studies, suggesting that hyperoside markedly reduces hepatic lipogenesis through the inhibition of ACC and SREBP-1. LXRα plays an important role in BAs and cholesterol metabolism, and up-regulation of SREBP-1 and CYP7A1 were observed in mice treated with LXR agonists [13]. Interestingly, we also noted that the expression of SREBP-1 critically depends on FXR agonists. When activated, FXR agonists can lead to the reduction of SREBP-1 expression [25,43,44]. In the present study, the protein expression of FXR and LXRα are both activated by hyperoside. Based on the results presented here, we raise the possibility that the dependence of the reduction of hepatic lipogenesis by hyperoside is mostly based on FXR, not LXRα.

FXR is deemed to play a significant role in the regulation of the cholesterol metabolism, BAs metabolism, and lipoprotein metabolism. It increases bile efflux via the induction of the BSEP expression/function, which regulates the excretion of BAs from the

hepatic cells into bile. In the present study, the protein level of BSEP in the hyperoside-treated rats is 1.44-fold higher than those in the model group, which is consistent with previous studies documenting that overexpressing of BSEP in mice leads to reduced hepatic steatosis when fed a lithogenic diet or a methionine choline-deficient (MCD) diet [45], most likely resulting from the activation of FXR. In addition, FXR can also increase the expression of multidrug resistance 3 (MDR3/ABCB4) which regulates the efflux of phospholipids into bile, and further protect the biliary epithelium from the toxicity of hydrophobic BAs [46]. In Table 1, we show that the hyperoside-treated rats had a 1.38-fold increase in protein expression of MDR3/ABCB4 compared with those in the model group. In short, our data likely exhibit a physiological reaction against TC and TG hepatic accumulation in the hyperoside-treated rats. In other words, the synthesis of TC and TG are inhibited; nevertheless, the secretion of BAs is elevated.

One of the interesting approaches to treating NAFLD is to increase fatty acid β-oxidation [47]. Our data show that proteins participating in fatty acid β-oxidation, including ECI1 and ACADSB, are up-regulated in rats feeding hyperoside in comparison with the model group, suggesting that fatty acid β-oxidation contributes to the TG-lowering action of hyperoside. FXR was also thought to enhance oxidation of fatty acids according to an extensive literature [20,25,48]. One of the mechanisms is that cholesterol efflux promotes the transfer of TC to lipid-poor apolipoproteins [49]. Apolipoproteins are responsible for plasma lipid transport and are major protein constituents of lipoproteins. Apolipoprotein E (ApoE) characterized by anti-inflammatory and antioxidative properties plays an important role in the packaging and secretion of HDL and VLDL to maintain hepatic lipid homoeostasis. ApoE
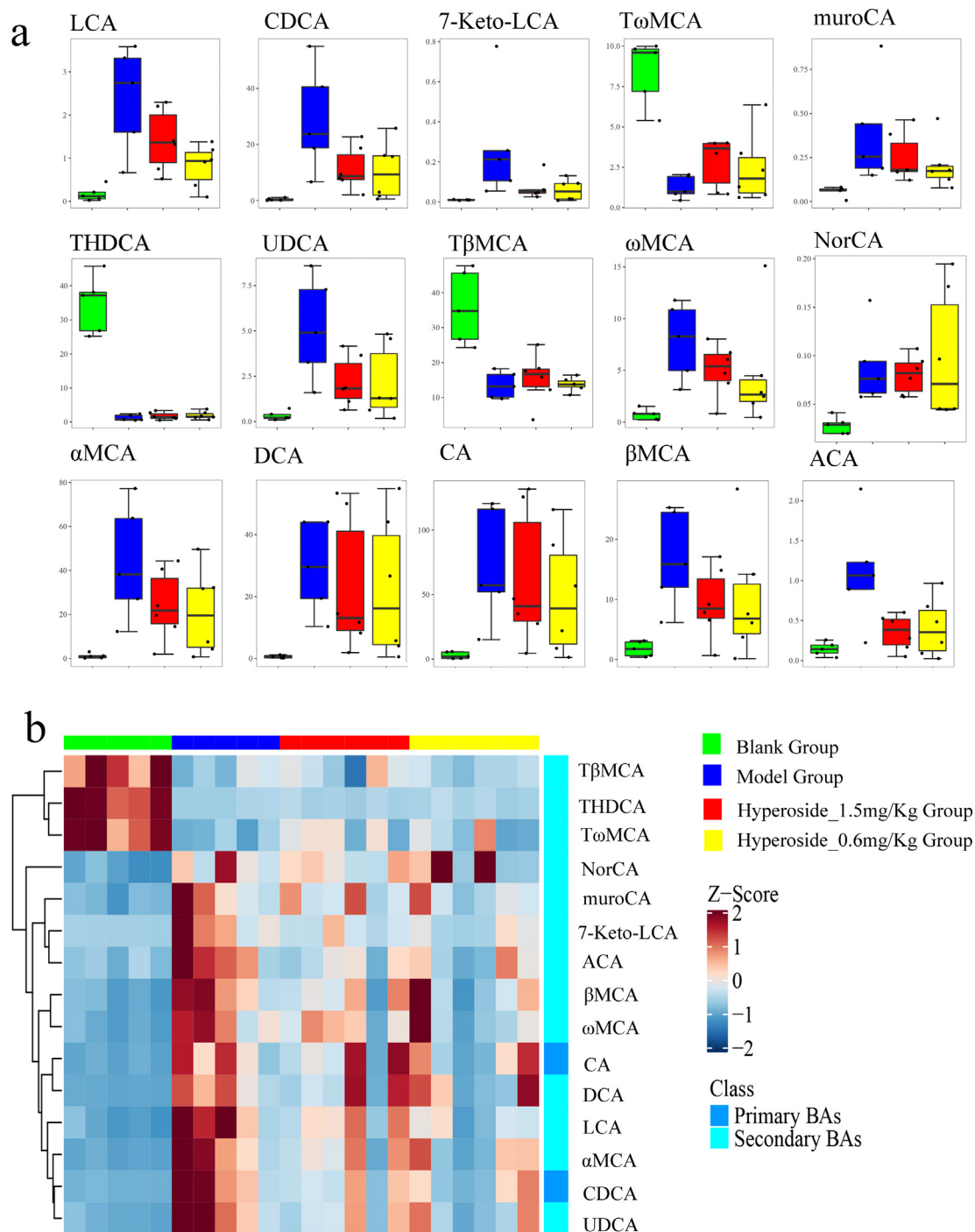
Fig. 5. The 15 BAs with significant contribution to the differentiation (a) The boxplot with points of 15 BAs with significant contribution to the differentiation ($p < 0.05$, Kruskal test); LCA, $p = 0.0045$, FDR = 0.0254; CDCA, $p = 0.0051$, FDR = 0.0254; 7-Keto-LCA, $p = 0.0057$, FDR = 0.0254; TωMCA, $p = 0.0069$, FDR = 0.0254; muroCA, $p = 0.0083$, FDR = 0.0254; THDCA, $p = 0.0084$, FDR = 0.0254; UDCA, $p = 0.0091$, FDR = 0.0254; TβMCA, $p = 0.0103$, FDR = 0.0254; ωMCA, $p = 0.0104$, FDR = 0.0254; NorCA, $p = 0.0111$, FDR = 0.0254; αMCA, $p = 0.0130$, FDR = 0.0272; DCA, $p = 0.0176$, FDR = 0.0337; CA, $p = 0.0226$, FDR = 0.0400; βMCA, $p = 0.0256$, FDR = 0.0420; ACA, $p = 0.0419$, FDR = 0.0642; FDR, false discovery rate (b) Heatmap with Z score of 15 BAs with significant contribution to the differentiation. The scale: blue colours indicate low Z values, whereas brown colours indicate high Z values.

deficiency in mice will lead to NAFLD in mice [50,51]. In our study, the protein expression of ApoC3 was induced by hyperoside, demonstrating that hyperoside alleviates NAFLD in rats by up-regulating ApoC3 as well. Since ApoC3 plays an intracellular role in the promotion of VLDL-TG secretion from the liver, elevated plasma ApoC3 levels are associated with increased production of hepatic VLDL-TG as well as decreased systemic clearance of TG-rich lipoproteins, contributing to hypertriglyceridemia develop-

ment [52], which is consistent with our previous research showing that hyperoside does not reduce serum TC and TG in rats, as shown in Fig S1c-d. In addition, the synthesis and secretion of apolipoproteins in the liver are also effected by FXR. FXR also regulates some key genes related to triglyceride metabolism (such as the microsomal triglyceride transfer protein and VLDL receptor) and apolipoproteins (C-II and C-III) [9,44] and the expression of ApoE can be also induced by LXRs [53]. Taking these results together,
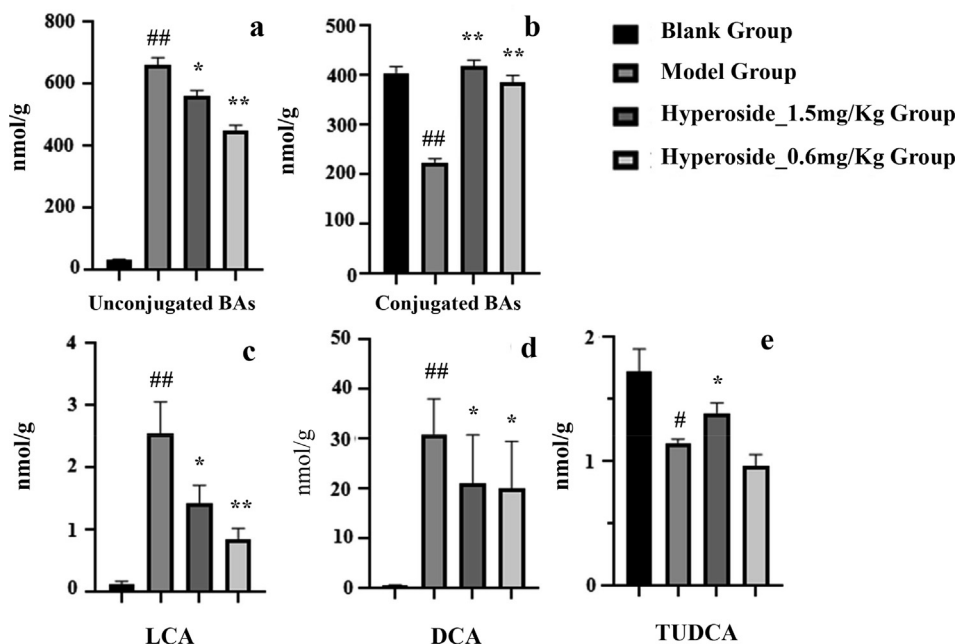
Fig. 6. Hyperoside treatment increases concentration of total conjugated BAs(b) and TUDCA(e), decreases the concentration of total unconjugated BAs(a), DCA(c), and LCA(d) in rat liver. Data are presented as mean ± SEM. ##, $p < 0.01$, #, $p < 0.05$, by unpaired Student t test compared with blank group, **, $p < 0.01$, *, $p < 0.05$, by unpaired Student t test compared with model group.

increasing FXR activity plays a significant role in the treatment of NAFLD rats by hyperoside. Besides, studies have also shown that FXR can be up-regulated by LXRα, which can be activated by 6α-hydroxy BAs as well as oxysterols [46,54].

In liver tissue, LXRα can promote the conversion of cholesterol into BAs since CYP7A1 is one of the direct gene targets of LXRα and its expression level depends upon LXRα in mice [18,55]. In this study, the protein expression levels of FXR and LXRα in rat feeding hyperoside are both markedly increased, together with the activation of CYP7A1 transcription [26,56]. However, FXR maintains cholesterol homeostasis by modulating CYP7A1 transcription via the negative feedback of the FXR-induced small heterodimer

partner (FXR-SHP) pathway, therefore limiting the cholesterol conversion to BAs [57]. The current result makes it plausible that LXRα, instead of FXR, is largely involved in the activation of CYP7A1 transcription in hyperoside-treated rats, promoting the conversion of cholesterol into BAs. Compared with the model group, the overexpression of CYP27A1 was more obvious than the CYP7A1 after the hyperoside treatment, indicating that the alternative BA synthesis pathway was activated as the main function target of hyperoside.

Disorders of lipid metabolism usually result from abnormal BA metabolisms, and hepatic lipid accumulation is one of important inducers of NAFLD [8,58]. In recent years, BAs regulation has been
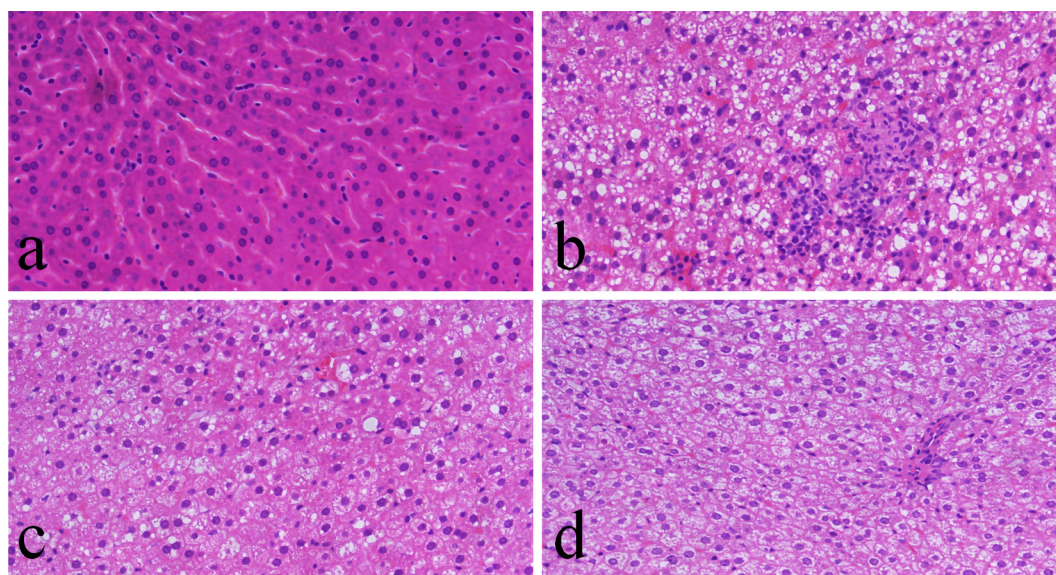
Fig. 7. Hepatic pathology of liver sections stained with Hematoxylin & eosin staining,(H&E)from (a) Blank group, (b) Model group, (c) Hyperoside_1.5 mg/Kg group, and (d) Hyperoside_0.6 mg/Kg group, to assess liver damage, original magnification, 200×.
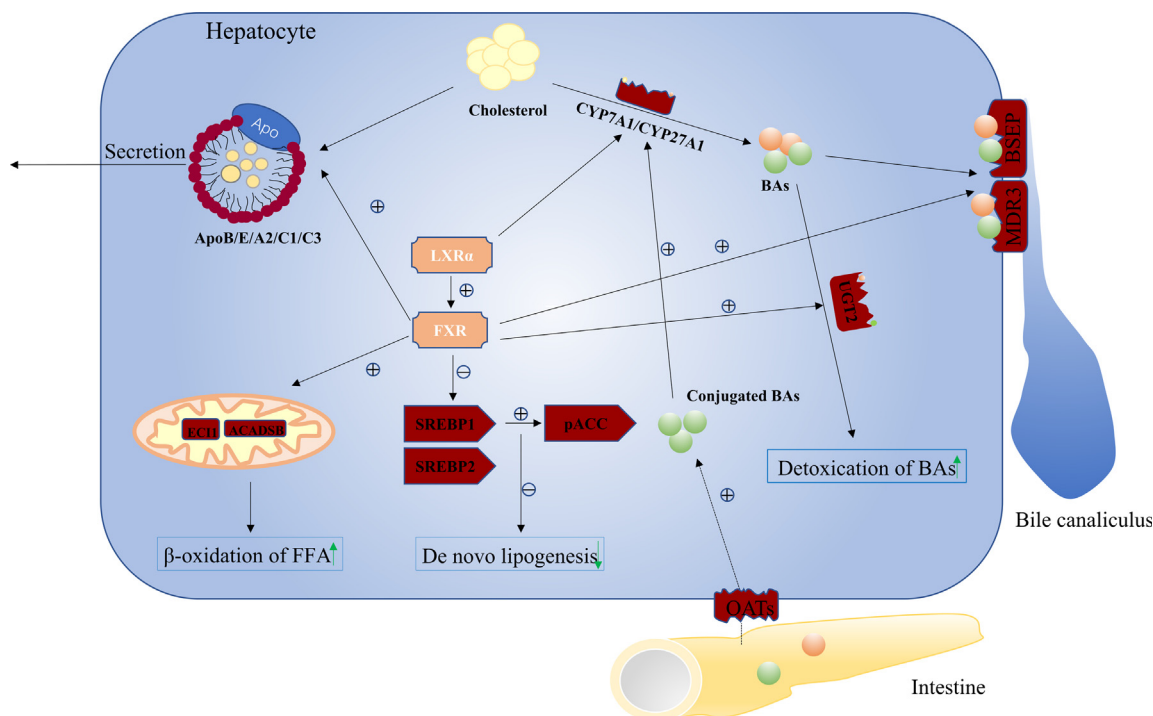
Fig. 8. The speculative mechanism of hyperoside for treatment of NAFLD in rats. Increased FXR expression is expected to increase the expression of UGT2, MDR3, BSEP, ECI1, ACADSB, and ApoB/E/AII/CI/CIII, and to decrease the expression of SREBP1. Enzymes BA synthesis is increased due to increased LXRα and conjugated BA level. OATs expression are also increased which would be expected to increase import of conjugated BA from intestine. ⊕, indicates up regulation; ⊖, indicates down regulation.

recognized as a novel therapeutic strategy for NAFLD treatment [59]. Altered hepatic BAs compositions signify the fact that liver attempts to reduce hepatotoxicity in progressive NAFLD. Besides, evidence of hydrophobic BAs toxicity is abundant, for example, increased exposure to hydrophobic BAs leads to the activation of necrosis and apoptosis pathways [60,61]. As shown in Fig. 6c–e, both concentration of DCA and LCA, the two most hydrophobic bile acids, have also shown a down-regulation in rats treated with hyperoside. In contrast, TUDCA which is more hydrophilic has been shown to protect organs against endoplasmic reticulum stress and oxidative [62], and is up-regulated in the hyperoside-treated rats. The results of HE staining in our study also suggest that the hyperoside reduces the inflammatory response in the rat's liver, might due to increased exposure to hydrophilic BAs and the overexpression of ApoE mentioned above. The HE staining is illustrated in Fig. 7. In addition, the low concentration levels of CA in hyperoside-treated rats reduce the assimilation of dietary cholesterol and fats, at the same time, improve the metabolism of glucose and lipid [62].

A high-fat diet causes the composition alteration of BAs, especially the secondary BAs and unconjugated BAs [38,63], which is also confirmed in this study. Conjugated BAs are more hydrophilic and show less cytotoxic effect compared with their unconjugated forms [64]. However, unconjugated BAs are risk factors for colon cancer due to the carcinogens [38]. Up-regulation of UGT2b10/35, an enzyme that catalyzes hydrophobic BAs into more hydrophilic glucuronide BAs, was observed in mice treated with hyperoside, suggesting that BAs conjugation is promoted. Furthermore, the promotion is associated with FXR activation [19].

The concentration levels of unconjugated BAs in the model group were increased significantly, about 20 times higher than in the blank group. Hyperoside consumption markedly decreased the concentration levels of the unconjugated BAs in the rats (p < 0.05, vs model group), accompanied by obviously increased concentration levels of conjugated BAs (p < 0.01, vs model group),

as shown in Fig. 6. Prior to secretion, BAs are mainly conjugated to taurine by the BA conjugation enzyme, bile acid coenzyme A: amino acid N-acyltransferase (BAAT), in the ileum of rats. Conjugated BAs are hydrolyzed into unconjugated BAs by bile salt hydrolase (BSH) enzymes that is produced in intestinal microbes [19,65]. Under normal circumstances, most BAs (95%) are recirculated to the liver by enterohepatic recycling, contributing approximately 5% of newly-synthesized BAs to the pool [6]. In the present proteomics research, BAAT does not represent an obvious increase in hyperoside-treated liver tissue (data were not shown). Accordingly, we speculate that high levels of conjugated BAs in hyperoside-treated livers might result from reduced BSH activity via decreased amounts of BSH-producing bacteria by hyperoside. The potential toxic effects induced by endogenous BAs could be ameliorated by the increased levels of conjugated BAs. In addition, emerging evidence suggest that the FXR-FGF15 signaling pathway in ileum can be restrained by the accumulation of intestinal conjugated BAs. Fibroblast growth factor 15 (FGF15) has been proved to activate the FGF receptor 4, resulting in the down-regulation of CYP7A1 expression and in the inhibition of BA synthesis in the liver [47,65,66]. We therefore deduce that elevated conjugated BAs in hyperoside-treated rat is also responsible for the up-regulation of CYP7A1 and CYP27A1, thereby promoting the synthesis of BAs in hepatic.

Conclusions

Collectively, our results indicate that the involved mechanisms by which hyperoside reduces lipid accumulation in a rat's liver are as follows: (1) increased conjugated BAs in the liver reducing the liver toxicity of endogenous unconjugated BAs and indirectly promoting conversion of cholesterol into BAs; (2) increased activation of liver FXR resulting in the promotion of the β-oxidation of free fatty acids along with decreased *de novo* lipogenesis; (3) increased cholesterol efflux and BAs excretion from the hepatocytes. The

speculative mechanisms are shown in Fig. 8. Up to now, no research focusing on the molecular mechanism by which hyperoside alleviates lipid accumulation in rats has been reported.

However, several gaps and limitations of this study need to be addressed in future. For example, details on hyperoside inhibiting both the gut microbiota (especially the one involved in BSH activity) and FXR-FGF15 signaling pathway in the rat's ileal are necessary to be further explored and validated. In addition, the optimal dosage of hyperoside requires clinical trials with large sample sizes. Our preliminary studies indicate that hyperoside is promising for the treatment of NAFLD in rats.

Compliance with Ethics Requirements

All Institutional and National Guidelines for the care and use of animals were followed.

CRediT authorship contribution statement

Songsong Wang: Methodology, Validation, Writing - original draft. **Feiya Sheng:** Methodology, Validation. **Liang Zou:** Methodology. **Jianbo Xiao:** Methodology, Writing - review & editing, Supervision, Project administration. **Peng Li:** Methodology, Writing - original draft, Writing - review & editing, Supervision, Project administration, Funding acquisition.

Declaration of Competing Interest

The authors have declared no conflict of interest

Acknowledgements

Appendix A. Supplementary data

Supplementary data to this article can be found online at https://doi.org/10.1016/j.jare.2021.06.001.

References

[1] Parker HM, Johnson NA, Burdon CA, Cohn JS, O'Connor HT, George J. Omega-3 supplementation and non-alcoholic fatty liver disease: a systematic review and meta-analysis. J Hepatol 2012;56(4):944–51.

[2] Browning JD, Szczepaniak LS, Dobbins R, Nuremberg P, Horton JD, Cohen JC, et al. Prevalence of hepatic steatosis in an urban population in the United States: impact of ethnicity. Hepatology 2004;40(6):1387–95.

[3] Angulo P. Obesity and Nonalcoholic Fatty Liver Disease. Nutr Rev 2007;65(6):57–63.

[4] Fang YL, Chen H, Wang CL, Liang L. Pathogenesis of non-alcoholic fatty liver disease in children and adolescence: From "two hit theory" to "multiple hit model". World J Gastroenterol 2018;24(27):2974–83.

[5] Liu Y, Li Q, Wang H, Zhao X, Li N, Zhang H, et al. Fish oil alleviates circadian bile composition dysregulation in male mice with NAFLD. J Nutr Biochem 2019;69:53–62.

[6] Tang Y, Zhang J, Li J, Lei X, Xu D, Wang Y, et al. Turnover of bile acids in liver, serum and caecal content by high-fat diet feeding affects hepatic steatosis in rats. Biochim Biophys Acta Mol Cell Biol Lipids 2019;1864(10):1293–304.

[7] Wahlstrom A, Sayin SI, Marschall HU, Backhed F. Intestinal Crosstalk between Bile Acids and Microbiota and Its Impact on Host Metabolism. Cell Metab 2016;24(1):41–50.

[8] Jiao N, Baker SS, Chapa-Rodriguez A, Liu W, Nugent CA, Tsompana M, et al. Suppressed hepatic bile acid signalling despite elevated production of primary and secondary bile acids in NAFLD. Gut 2018;67(10):1881–91.

[9] Arab JP, Karpen SJ, Dawson PA, Arrese M, Trauner M. Bile acids and nonalcoholic fatty liver disease: Molecular insights and therapeutic perspectives. Hepatology 2017;65(1):350–62.

[10] Leung C, Rivera L, Furness JB, Angus PW. The role of the gut microbiota in NAFLD. Nat Rev Gastroenterol Hepatol 2016;13(7):412–25.

[11] Rinella ME, Sanyal AJ. NAFLD in 2014: Genetics, diagnostics and therapeutic advances in NAFLD. Nat Rev Gastroenterol Hepatol 2015;12(2):65–6.

[12] Li H, Xi Y, Xin X, Tian H, Hu Y. Salidroside improves high-fat diet-induced non-alcoholic steatohepatitis by regulating the gut microbiota-bile acid-farnesoid X receptor axis. Biomed Pharmacother 2020;124:109915.

[13] Schultz JR, Tu H, Luk A, Repa JJ, Medina JC, Li L, et al. Role of LXRs in control of lipogenesis. Genes Dev 2020;14:9.

[14] Fiorucci S, Rizzo G, Donini A, Distrutti E, Santucci L. Targeting farnesoid X receptor for liver and metabolic disorders. Trends Mol Med 2007;13(7):298–309.

[15] Musso G, Gambino R, Cassader M. Cholesterol metabolism and the pathogenesis of non-alcoholic steatohepatitis. Prog Lipid Res 2013;52(1):175–91.

[16] Rana R, Shearer AM, Fletcher EK, Nguyen N, Guha S, Cox DH, et al. PAR2 controls cholesterol homeostasis and lipid metabolism in nonalcoholic fatty liver disease. Mol Metab 2019;29:99–113.

[17] Kawano Y, Cohen DE. Mechanisms of hepatic triglyceride accumulation in non-alcoholic fatty liver disease. J Gastroenterol 2013;48(4):434–41.

[18] Peter HRK, Edwards A, Anisfeld AM. BAREing it all: the adoption of LXR and FXR and their roles in lipid homeostasis. J Lipid Res 2002;43:11.

[19] Zhang Y, Edwards PA. FXR signaling in metabolic disease. FEBS Lett 2008;582(1):10–8.

[20] Savkur RS, Bramlett KS, Michael LF, Burris TP. Regulation of pyruvate dehydrogenase kinase expression by the farnesoid X receptor. Biochem Biophys Res Commun 2005;329(1):391–6.

[21] Vlahcevic ZR, Pandak WM, Heuman DM, Hylemon PB. Function and Regulation of Hydroxylases Involved in the Bile Acid Biosynthesis Pathways. Semin Liver Dis 1992;12(4):17.

[22] Fuchs C, Claudel T, Trauner M. Bile acid-mediated control of liver triglycerides. Semin Liver Dis 2013;33(4):330–42.

[23] Li T, Chiang JY. Bile acid signaling in metabolic disease and drug therapy. Pharmacol Rev 2014;66(4):948–83.

[24] Goedeke L, Bates J, Vatner DF, Perry RJ, Wang T, Ramirez R, et al. Acetyl-CoA Carboxylase Inhibition Reverses NAFLD and Hepatic Insulin Resistance but Promotes Hypertriglyceridemia in Rodents. Hepatology 2018;68(6):2197–211.

[25] Watanabe M, Houten SM, Wang L, Moschetta A, Mangelsdorf DJ, Heyman RA, et al. Bile acids lower triglyceride levels via a pathway involving FXR, SHP, and SREBP-1c. J Clin Invest (10) 2004:12.

[26] Liu S, Wu Z, Guo S, Meng X, Chang X. Polyphenol-rich extract from wild Lonicera caerulea berry reduces cholesterol accumulation by mediating the expression of hepatic miR-33 and miR-122, HMGCR, and CYP7A1 in rats. J Funct Foods 2018;40:648–58.

[27] Van Rooyen DM, Larter CZ, Haigh WG, Yeh MM, Ioannou G, Kuver R, et al. Hepatic free cholesterol accumulates in obese, diabetic mice and causes nonalcoholic steatohepatitis. Gastroenterology 2011;141(4):1393–403. 1403 e1-5.

[28] Michael JLG, Brown S. The SREBP Pathway: Regulation of Cholesterol Metabolism by Proteolysis of a Membrane-Bound Transcription Factor. Cell 1997;89(3):331.

[29] Shimano H, Horton JD, Shimomura I, Hammer RE, Brown MS, Goldstein JL. Isoform 1c of sterol regulatory element binding protein is less active than isoform 1a in livers of transgenic mice and in cultured cells. J Clin Invest 1997;99(5):846–54.

[30] Yang J, Qian D, Guo J, Jiang S, Shang EX, Duan JA, et al. Identification of the major metabolites of hyperoside produced by the human intestinal bacteria using the ultra performance liquid chromatography/quadrupole-time-of-flight mass spectrometry. J Ethnopharmacol 2013;147(1):174–9.

[31] Raza A, Xu X, Sun H, Tang J, Ouyang Z. Pharmacological activities and pharmacokinetic study of hyperoside: A short review. Trop J Pharm Res 2017;16(2):483.

[32] Li L, Bebek G, Previs SF, Smith JD, Sadygov RG, McCullough AJ, et al. Proteome Dynamics Reveals Pro-Inflammatory Remodeling of Plasma Proteome in a Mouse Model of NAFLD. J Proteome Res 2016;15(9):3388–404.

[33] Kampf C, Mardinoglu A, Fagerberg L, Hallstrom BM, Edlund K, Lundberg E, et al. The human liver-specific proteome defined by transcriptomics and antibody-based profiling. FASEB J 2014;28(7):2901–14.

[34] Bell LN, Theodorakis JL, Vuppalanchi R, Saxena R, Bemis KG, Wang M, et al. Serum proteomics and biomarker discovery across the spectrum of nonalcoholic fatty liver disease. Hepatology 2010;51(1):111–20.

[35] Niu L, Geyer PE, Wewer Albrechtsen NJ, Gluud LL, Santos A, Doll S, et al. Plasma proteome profiling discovers novel proteins associated with non-alcoholic fatty liver disease. Mol Syst Biol 2019;15(3):e8793.

[36] Zhang YP, Deng YJ, Tang KR, Chen RS, Liang S, Liang YJ, et al. Berberine Ameliorates High-Fat Diet-Induced Non-Alcoholic Fatty Liver Disease in Rats via Activation of SIRT3/AMPK/ACC Pathway. Curr Med Sci 2019;39(1):37–43.

[37] Zhu Y, Xu H, Chen H, Xie J, Shi M, Shen B, et al. Proteomic analysis of solid pseudopapillary tumor of the pancreas reveals dysfunction of the endoplasmic reticulum protein processing pathway. Mol Cell Proteomics 2014;13(10):2593–603.

[38] Wan Y, Yuan J, Li J, Li H, Zhang J, Tang J, et al. Unconjugated and secondary bile acid profiles in response to higher-fat, lower-carbohydrate diet and associated

with related gut microbiota: A 6-month randomized controlled-feeding trial. Clin Nutr 2020;39(2):395–404.

[39] Liu XJ, Liu C, Zhu LY, Fan CL, Niu C, Liu XP, et al. Hepalatide ameliorated progression of nonalcoholic steatohepatitis in mice. Biomed Pharmacother 2020;126:110053.

[40] Tong L, Harwood Jr HJ. Acetyl-coenzyme A carboxylases: versatile targets for drug discovery. J Cell Biochem 2006;99(6):1476–88.

[41] Kawaguchi T, Ueno T, Nogata Y, Hayakawa M, Koga H, Torimura T. Wheat-bran autolytic peptides containing a branched-chain amino acid attenuate non-alcoholic steatohepatitis via the suppression of oxidative stress and the upregulation of AMPK/ACC in high-fat diet-fed mice. Int J Mol Med 2017;39 (2):407–14.

[42] Fang K, Wu F, Chen G, Dong H, Li J, Zhao Y, et al. Diosgenin ameliorates palmitic acid-induced lipid accumulation via AMPK/ACC/CPT-1A and SREBP-1c/FAS signaling pathways in LO2 cells. BMC Complement Altern Med 2019;19 (1):255.

[43] Zhang Y, Castellani LW, Sinal CJ, Gonzalez FJ, Edwards PA. Peroxisome proliferator-activated receptor-gamma coactivator 1alpha (PGC-1alpha) regulates triglyceride metabolism by activation of the nuclear receptor FXR. Genes Dev 2004;18(2):157–69.

[44] Carr RM, Reid AE. FXR agonists as therapeutic agents for non-alcoholic fatty liver disease. Curr Atheroscler Rep 2015;17(4):500.

[45] Fuchs CD, Krivanec S, Steinacher D, Mlitz V, Wahlstrom A, et al. Absence of Bsep/Abcb11 attenuates MCD diet-induced hepatic steatosis but aggravates inflammation in mice. Liver Int 2020;40(6):1366–77.

[46] Enjoji M, Yada R, Fujino T, Yoshimoto T, Yada M, Harada N, et al. The state of cholesterol metabolism in the liver of patients with primary biliary cirrhosis: the role of MDR3 expression. Hepatol Int 2009;3(3):490–6.

[47] Fuchs CD, Traussnigg SA, Trauner M. Nuclear Receptor Modulation for the Treatment of Nonalcoholic Fatty Liver Disease. Semin Liver Dis 2016;36 (1):69–86.

[48] Paschos PK, Non P. Alcoholic fatty liver disease and metabolic syndrome. HIPPOKRATIA 2009;13(1):11.

[49] Francisco Blanco-Vaca JCE-G, Martín-Campos Jesús M, Julve Josep. Role of apoA-II in lipid metabolism and atherosclerosis: advances in the study of an enigmatic protein. J Lipid Res 2001;42:13.

[50] Lu W, Mei J, Yang J, Wu Z, Liu J, Miao P, et al. ApoE deficiency promotes non-alcoholic fatty liver disease in mice via impeding AMPK/mTOR mediated autophagy. Life Sci 2020;252:117601.

[51] Zhang Z, Zong C, Jiang M, Hu H, Cheng X, Ni J, et al. Hepatic HuR modulates lipid homeostasis in response to high-fat diet. Nat Commun 2020;11(1):3067.

[52] Cheng X, Yamauchi J, Lee S, Zhang T, Gong Z, Muzumdar R, et al. APOC3 Protein Is Not a Predisposing Factor for Fat-induced Nonalcoholic Fatty Liver Disease in Mice. J Biol Chem 2017;292(9):3692–705.

[53] Jiang Q, Lee CY, Mandrekar S, Wilkinson B, Cramer P, Zelcer N, et al. ApoE promotes the proteolytic degradation of Abeta. Neuron 2008;58(5):681–93.

[54] Peter ES, Jansen LM. Genetic cholestasis, causes and consequences for hepatobiliary transport. Liver Int 2003;23:8.

[55] Calkin AC, Tontonoz P. Transcriptional integration of metabolism by the nuclear sterol-activated receptors LXR and FXR. Nat Rev Mol Cell Biol 2012;13 (4):213–24.

[56] Liang YT, Chen J, Jiao R, Peng C, Zuo Y, Lei L, et al. Cholesterol-Lowering Activity of Sesamin Is Associated with Down-Regulation on Genes of Sterol Transporters Involved in Cholesterol Absorption. J Agric Food Chem 2015;63 (11):2963–9.

[57] Dávalos A, Fernández-Hernando C. From evolution to revolution: miRNAs as pharmacological targets for modulating cholesterol efflux and reverse cholesterol transport. Pharmacol Res 2013;75:60–72.

[58] Buzzetti E, Pinzani M, Tsochatzis EA. The multiple-hit pathogenesis of non-alcoholic fatty liver disease (NAFLD). Metabolism 2016;65(8):1038–48.

[59] Yu Q, Jiang Z, Zhang L. Bile acid regulation: A novel therapeutic strategy in non-alcoholic fatty liver disease. Pharmacol Ther 2018;190:81–90.

[60] Horvatits T, Trauner M, Fuhrmann V. Hypoxic liver injury and cholestasis in critically ill patients. Curr Opin Crit Care 2013;19(2):128–32.

[61] Lake AD, Novak P, Shipkova P, Aranibar N, Robertson D, Reily MD, et al. Decreased hepatotoxic bile acid composition and altered synthesis in progressive human nonalcoholic fatty liver disease. Toxicol Appl Pharmacol 2013;268(2):132–40.

[62] Chiang JYL. Bile acid metabolism and signaling in liver disease and therapy. Liver Res 2017;1(1):3–9.

[63] He X, Ji G, Jia W, Li H. Gut Microbiota and Nonalcoholic Fatty Liver Disease: Insights on Mechanism and Application of Metabolomics. Int J Mol Sci 2016;17 (3):300.

[64] Alan M, Hofmann F. The Continuing Importance of Bile Acids in Liver and Intestinal Disease. Arch Intern Med 1999;159:12.

[65] Huang F, Zheng X, Ma X, Jiang R, Zhou W, Zhou S, et al. Theabrownin from Pu-erh tea attenuates hypercholesterolemia via modulation of gut microbiota and bile acid metabolism. Nat Commun 2019;10(1):4971.

[66] Uriarte I, Fernandez-Barrena MG, Monte MJ, Latasa MU, Chang HC, Carotti S, et al. Identification of fibroblast growth factor 15 as a novel mediator of liver regeneration and its application in the prevention of post-resection liver failure in mice. Gut 2013;62(6):899–910.